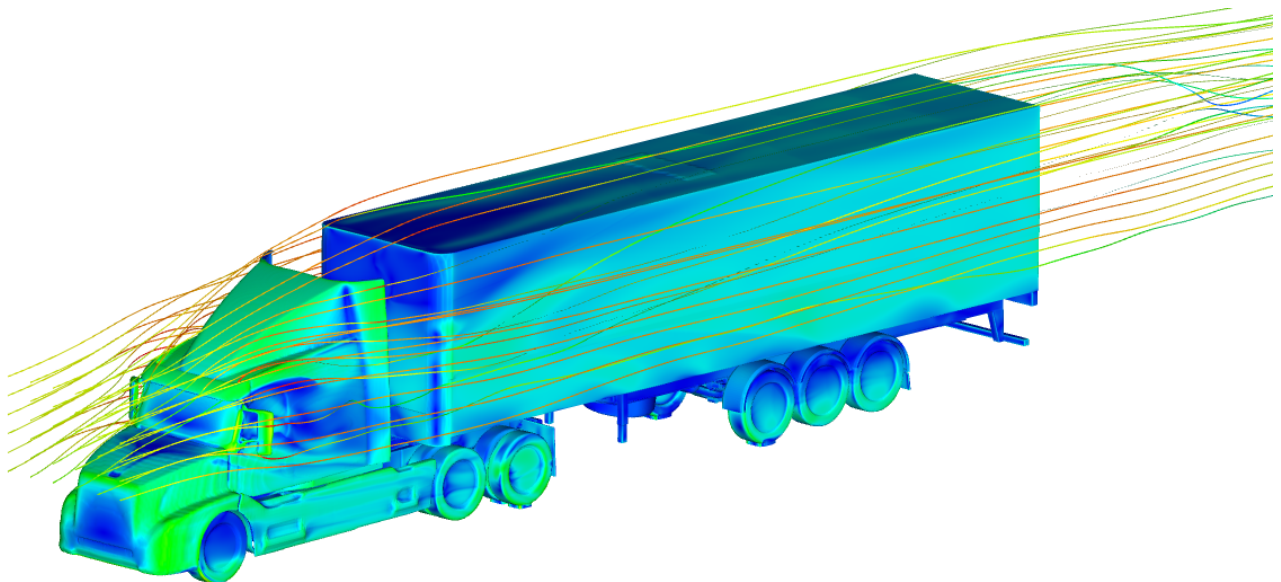


CHALMERS



Numerical Simulations of the Flow around a Yawing Truck in Wind Tunnel

Master's thesis in Automotive Engineering

XINKE MU

Department of Applied Mechanics
Division of Fluid Mechanics
CHALMERS UNIVERSITY OF TECHNOLOGY
Göteborg, Sweden 2011
Master's thesis 2011:63

MASTER'S THESIS IN AUTOMOTIVE ENGINEERING

Numerical Simulations of the Flow around a Yawing Truck in Wind Tunnel

XINKE MU

Department of Applied Mechanics
Division of Fluid Mechanics
CHALMERS UNIVERSITY OF TECHNOLOGY
Göteborg, Sweden 2011

Numerical Simulations of the Flow around a Yawing Truck in Wind Tunnel

XINKE MU

© XINKE MU, 2011

Master's thesis in Automotive Engineering 2011:63

ISSN 1652-8557

Department of Applied Mechanics

Division of Fluid Mechanics

Chalmers University of Technology

SE-412 96 Göteborg

Sweden

Telephone: +46 (0)31-772 1000

Cover:

$k - \zeta - f$ simulation result of the flow around a truck in wind tunnel. Visualizing resolved stream lines. Streamline and truck colored by velocity magnitude.

Chalmers Reproservice

Göteborg, Sweden 2011

Numerical Simulations of the Flow around a Yawing Truck in Wind Tunnel

Master's thesis in Automotive Engineering

XINKE MU

Department of Applied Mechanics

Division of Fluid Mechanics

Chalmers University of Technology

ABSTRACT

Ground vehicles such as cars and heavy trucks travelling on road are often exposed to unsteady flows. Particularly, the oscillation of vehicles in the vertical direction (maybe caused by side force from being subjected to strong gusty wind, or bumpy road) can produce time-dependent flow condition. This kind of transient force also occurs in the experiment tests with a rotating vehicle for getting variable yaw angle. Although the oscillation speed in the experiment is fairly low, however the unsteady flow conditions can lead to an intersection between the flow and vehicle movement. This intersection thus will change how the aerodynamic forces and moments will be developed. Therefore, in order to study the effects of vehicle oscillation on flow development and predict the aerodynamic force at steady condition, both steady and transient dynamic simulation were conducted. All simulations are based on the experiment scenario carried out with a Volvo heavy truck in the RUAG wind tunnel. However, the oscillation frequency in the experiment is too low, so a higher oscillation frequency was adopted in the transient dynamic simulation in order to accomplish the simulation in a reasonable time. $k - \zeta - f$ eddy-viscosity turbulence model were adopted in all steady and transient simulation due to its accuracy and robustness at high Reynolds number ($Re = 6.68 * 10^6$) Surface meshes were repaired and modified in ANSA and AVL-Fire, volume meshes were generated using FAMEHexa provided by AVL List GmbH, and AVL-Fire were used as the CFD solver.

For the steady simulations, drag, yaw moment and flow field were estimated for 0 and 5 degree yaw angle. For the transient dynamic simulation, mesh deformation method was used to simulate the vehicle's yaw movement. The oscillation frequency of $f = 2Hz$ was chosen to correspond to the Strouhal number $St = fL/U_\infty = 0.18$.

Keywords: CFD, $k - \zeta - f$, truck, oscillation

PREFACE

This master thesis has simulated the air flow around a half-scaled Volvo truck including a tractor and a semitrailer in the RUAG wind tunnel. Drag and yaw moment at different yaw angles were estimated both in steady case and dynamic case. The original surface mesh was provided by Volvo 3P. Surface mesh was repaired and modified in ANSA and AVL-Fire. FAMEHexa was used for generating volume meshes, and AVL-Fire was used as CFD solver. This project was carried out from February 2011 to September 2011 at the Department of Applied Mechanics, Division of Fluid Dynamics, Chalmers University of Technology, Sweden, by Xinke Mu. This Master's Thesis Project has been supervised and examined by Associate Professor Sinisa Krajnovic from Chalmers and Zenitha Chroner from Volvo 3P.

ACKNOWLEDGEMENTS

This project has been through a hard but meaningful time. First I would like to thank Jurgen Schneider, Bojan Krajnc, Peter Sampl and Albert Vander Meer at AVL List GmbH for their valuable technical support. I am also grateful to Per Ringquist, Ragnar Larusson, Jan Östh, Xingsi Han and other colleagues at Fluid Dynamics Division of Chalmers. I have learned a lot from them both about technical knowledges and about life. I also would like to thank AVL List GmbH for providing software license, and NSC (National Supercomputer Centre) at Linköping University, Sweden, and C3SE (Centre for Scientific and Technical Computing) at Chalmers University of Technology, Sweden, for providing computer access.

Sincerely, I would like to thank my supervisors, Associate Professor Sinisa Krajnovic and Zenitha Chroner Ph.D Analysis Engineer CFD at Volvo 3P for their guide and support throughout the project.

Finally, I would like to thank my parents, my families. Without them, there's no way I can go so far.

Contents

Abstract	i
Preface	iii
Acknowledgements	iii
Contents	v
1 Introduction	1
1.1 Background	1
1.2 Previous work	2
1.3 Purpose	3
1.4 Limitations	3
2 Theory	4
2.1 Governing equation	4
2.1.1 Time-averaged governing equation	4
2.1.2 $k - \zeta - f$ turbulence model	5
2.2 Aerodynamic Coefficient	5
2.3 CFD Coefficient	6
2.4 Hybrid wall treatment	6
3 Method	8
3.1 The wind tunnel experiment	8
3.1.1 RAUG wind tunnel	8
3.1.2 Experiment setup	8
3.2 Computational domain	9
3.3 Meshes	10
3.4 Boundary condition and numerical setup	12
3.4.1 Boundary condition and initial condition	12
3.4.2 Simulations	12
3.4.3 Numerical setup for CFD solver	13
4 Results	14
4.1 Wind tunnel experiment data analysis with CFD results	14
4.2 Numerical simulation results for stationary truck at 0° and 5° yaw angle	16
4.2.1 Overview of the flow field	16
4.2.2 Flow in the gap between tractor and trailer	21
4.2.3 Underbody flow	23
4.3 Comparison between stationary and rotating cases	25
5 Discussion and Conclusion	32

1 Introduction

1.1 Background

Aerodynamic forces and flow field around a ground vehicle exposed to crosswind has been an interest for many researchers, since transient response and crosswind stability are important issues for both aerodynamic performance and safety aspects. The most common approach in studies of crosswind effects is to evaluate the aerodynamic performance using static conditions. The experiment or the simulation is then made for one position at a time. Such experimental studies or numerical simulations are called “quasi-steady”. However, tests using dynamic flow conditions have shown different forces and moment from those found in steady flow conditions. Hysteresis effects and a phase shift in forces and moment have also been observed. This difference causes uncertainty to some experiment data, for instance, the drag force and yaw moment measurement of a slowly rotating truck in a wind tunnel, see Figure 1.1.1.



Figure 1.1.1: *An oscillating half-scaled Volvo truck in the RUAG wind tunnel.*

The air flow around a vehicle exposed to crosswind at high Reynolds number, is highly turbulent and transient. Therefore, a time-dependent numerical method such as LES, PANS and URANS should be adopted. Reynolds Averaged Navier Stokes (RANS) models is a computationally cheap method of computing turbulent flows, but it is computing only the time average of the flow. Large Eddy Simulations (LES), is a method that is superior to RANS model in strongly separated flow. For example with wake flow, LES simulates directly the large turbulent structures and models only the influence of the sub-grid scales on the resolved ones. However, LES has high computational costs, since it demands very fine resolution of mesh, particularly in the attached boundary region. Partially Averaged Navier Stokes (PANS) models is another alternative recently proposed by Girimaji [1]. PANS offers a way to regulate the amount of time averaging in the RANS-equations, making it possible to resolve a desired amount of the turbulent fluctuations, as well as having a good model for the unresolved scales. PANS is however less established than LES, and ongoing research is evaluating its capabilities. Unsteady Reynolds Averaged Navier Stokes (URANS) model also is able to predict transient flow. Since it resolves only unsteady, mean flow structures which are primarily larger than the turbulent eddies, it is fairly computational cheap, and thus is able to simulate industrial applications with complex geometry and large amount of mesh cells.

1.2 Previous work

Tests using dynamic flow conditions have shown different forces and moment from those found in steady flow conditions; hysteresis effects and a phase shift in force and moment signals were also observed.

An experimental investigation was conducted by Grillieron et al. (2003) [2] to study the flow around a simplified ground vehicle model pitching around a horizontal axis. The body used in their study was cylindrical with its front shaped as a Rankine half-oval, and its rear base inclined at an pitching angle of 43° . Their experimental results showed the existence of a hysteresis phenomenon and a phase shift in the surface pressure signal. Passmore and Mansor (2006) conduct an experimental study on a simplified vehicle (a Davis model) which was constrained to oscillate with a single degree of freedom of yawing motion in a steady flow stream. Large differences between dynamic and quasi-steady tests were found.

Watkins and Saunders [3] have shown that the range of frequencies of importance in crosswind studies is 0.2-2.0Hz, corresponding to $St=0.09-0.9$.

Recently, Krajnovic et al. [4] have shown that transient CFD simulation such as large eddy simulation (LES) can predict the real dynamic flow conditions around generic vehicles under the influence of wind gusts and explain the differences in the results between the dynamic and quasi-steady tests. Their LES simulations modeled the flow around a simplified vehicle model oscillating around its vertical axis at the frequency of $St = 0.068$. Mesh deformation method was used to simulate the yaw movement of the vehicle. Their results were found to agree well with the previous experimental investigation, and the phenomena of hysteresis and phase shift for aerodynamic forces and moment can be observed in Figure 1.2.1. Furthermore, the cause of the phenomena of hysteresis and phase shift was revealed to be in the inertia of the flow to adjust to sudden changes in the direction of the oscillation of the vehicle body.

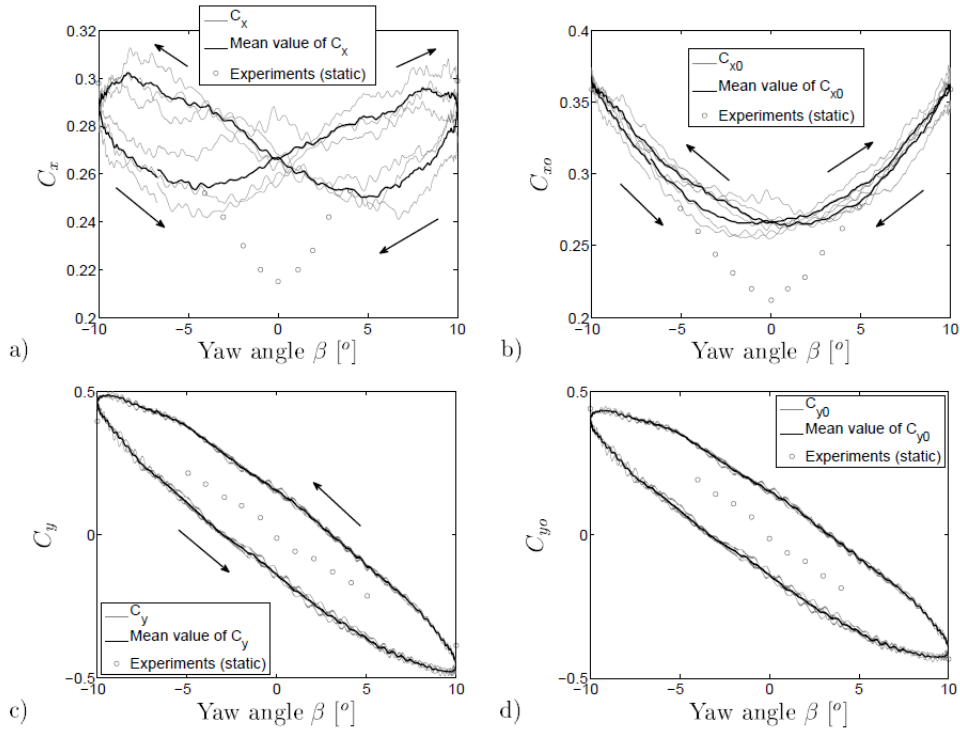


Figure 1.2.1: Comparison of the a) drag coefficient C_x ; b) drag coefficient calculated in the Eiffel axis linked to the upstream velocity U_{infty} , C_{x0} ; c) side force coefficient C_y ; and d) side force coefficient linked to the Eiffel axis C_{y0} . From Krajnovic et al. [4]

1.3 Purpose

This project aims to use time-dependent numerical simulations URANS and steady RANS with $k - \zeta - f$ model to study the flow around VOLVO truck exposed to both steady and dynamic flow conditions. The difference of the flow field and thereby the aerodynamics performance at steady and dynamic condition is explored. Furthermore, the drag coefficient and the flow are predicted for different yaw angles.

1.4 Limitations

Due to the complexity of the geometry, in order to get quality-acceptable cells and limited number of cells, the truck model simulated was slightly smoothed and modified from the real model in the experiment. However, the effect on results of this modification was ignored. To finish the simulation within a reasonable short time, a higher oscillating frequency was used rather the very low frequency used in the experiment. Due to lack of time and computational power, 33m/s inlet speed are used in the dynamic simulation and the compared steady simulation. 50m/s inlet speed are used in the steady simulation for drag prediction.

2 Theory

In this section, all basic theories behind the simulations in this project are presented, including turbulence modelling, coefficient, and wall treatment.

2.1 Governing equation

All fluid motions are governed by the famous Navier-Stokes (NS) equation. For the incompressible flow with constant viscosity, the NS equation is described as :

$$\frac{\partial U_i}{\partial t} + U_j \frac{\partial U_i}{\partial x_j} = -\frac{\partial P}{\partial x_i} + \nu \frac{\partial^2 U_i}{\partial x_j \partial x_j} \quad (2.1.1)$$

Where U_i is the velocity, P is the pressure and ν is the kinematic viscosity. Also $\nu = \mu/\rho$, where μ is the dynamical viscosity and ρ is the fluid density. By keeping mass conservation for incompressible flow, continuity equation can be derived as:

$$\frac{\partial U_i}{\partial x_i} = 0 \quad (2.1.2)$$

2.1.1 Time-averaged governing equation

Assuming a complete set of boundary conditions being available, there are four unknowns in Navier-Stokes (NS) equations and continuity equation, thus the system of equations can be directly solved. This approach is called Direct Numerical Simulation (DNS), and it can solve turbulences at all scales. However, it's too expensive to be used in industrial applications, and additionally in most cases, the turbulence is of secondary interest, but its effect on the mean flow characteristics and the subjected body is our major concern. Therefore when solving the Navier-Stokes equations, the instantaneous variables can be decomposed into a mean component and a fluctuating component as described below:

$$U_i = \bar{U}_i + u'_i, \quad (2.1.3)$$

where the bar, $\bar{\cdot}$, denotes the time averaged value. Inserting Eq. 2.1.3 into the continuity equation (2.1.2) and the Navier-Stokes equation (2.1.1) we obtain the time averaged continuity equation and Navier-Stokes equation:

$$\frac{\partial \bar{U}_i}{\partial x_i} = 0 \quad (2.1.4)$$

$$\rho \frac{\partial \bar{U}_i}{\partial t} + \rho \frac{\partial \bar{U}_i \bar{U}_j}{\partial x_j} = -\frac{\partial \bar{p}}{\partial x_i} + \frac{\partial}{\partial x_j} \left(\mu \frac{\partial \bar{U}_i}{\partial x_j} - \rho \overline{u'_i u'_j} \right) \quad (2.1.5)$$

This equation is the time-averaged Navier-Stokes equation and it is often called the Reynolds equation. A new term ρv_{ij} appears on the right side of Eq. 2.1.5 which is called the Reynolds stress tensor. The tensor is symmetric (for example $\overline{u'_1 u'_2} = \overline{u'_2 u'_1}$). It represents correlations between fluctuating velocities. It is an additional stress term due to turbulence (fluctuating velocities) and it is unknown. We need a model for v_{ij} to close the equation system in Eq. 2.1.5. This is called the closure problem: the number of unknowns (ten: three velocity components, pressure, six stresses) is larger than the number of equations (four: the continuity equation and three components of the Navier-Stokes equations).

2.1.2 $k - \zeta - f$ turbulence model

When performing calculations using the time-averaged Navier-Stokes equations the turbulence may be modelled using the $\zeta - f$ eddy-viscosity turbulence model presented in [5]. The essential part of the turbulence model is that a transport equation for the velocity scale ratio, $\zeta = \frac{\bar{v}^2}{k}$, is solved and an elliptic damping function, f , is used. The turbulent viscosity is defined in equation 2.1.6.

$$\nu_t = C_\mu \zeta k \tau \quad (2.1.6)$$

The transport equations are

$$\frac{\partial k}{\partial t} + \bar{u}_j \frac{\partial k}{\partial x_j} = \frac{1}{\rho} \frac{\partial}{\partial x_j} \left[\left(\mu + \frac{\mu_t}{\sigma_k} \right) \frac{\partial k}{\partial x_j} \right] + P_k - \varepsilon \quad (2.1.7)$$

$$\frac{\partial \varepsilon}{\partial t} + \bar{u}_j \frac{\partial \varepsilon}{\partial x_j} = \frac{1}{\rho} \frac{\partial}{\partial x_j} \left[\left(\mu + \frac{\mu_t}{\sigma_\varepsilon} \right) \frac{\partial \varepsilon}{\partial x_j} \right] + \frac{1}{\tau} [C_{\varepsilon 1}^* P_k - C_{\varepsilon 2} \varepsilon] \quad (2.1.8)$$

$$\frac{\partial \zeta}{\partial t} + \bar{u}_j \frac{\partial \zeta}{\partial x_j} = \frac{1}{\rho} \frac{\partial}{\partial x_j} \left[\left(\mu + \frac{\mu_t}{\sigma_\zeta} \right) \frac{\partial \zeta}{\partial x_j} \right] + f - P_k \frac{\zeta}{k} \quad (2.1.9)$$

The damping function f is obtained by solving 2.1.10

$$L^2 \frac{\partial^2 f}{\partial x_j \partial x_j} - f = \left(C_{f1} + C_{f2} \frac{P_k}{\varepsilon} \right) \left(\zeta - \frac{2}{3} \right) \frac{1}{\tau} \quad (2.1.10)$$

The turbulent time scale τ and length scale L are given by

$$\tau = \max \left[\min \left[\frac{k}{\varepsilon}, \frac{0.6}{\sqrt{6} C_\mu |S| \zeta} \right], C_\tau \left(\frac{\nu}{\varepsilon} \right)^{1/2} \right] \quad (2.1.11)$$

$$L = C_L \max \left[\min \left[\frac{k^{3/2}}{\varepsilon}, \frac{k^{1/2}}{\sqrt{6} C_\mu |S| \zeta} \right], C_\eta \left(\frac{\nu^3}{\varepsilon} \right)^{1/4} \right] \quad (2.1.12)$$

The coefficient $C_{\varepsilon 1}^*$ is modified in the ε equation by dampening it near the wall using 2.1.13

$$C_{\varepsilon 1}^* = C_{\varepsilon 1} (1 + 0.012/\zeta) \quad (2.1.13)$$

The values of the coefficients for the $\zeta - f$ model is shown in Table 2.1.1.

Table 2.1.1: *Coefficients for the $\zeta - f$ model.*

C_μ	$C_{\varepsilon 1}$	$C_{\varepsilon 2}$	C_{f1}	C_{f2}	σ_k	σ_ε	σ_ζ	C_τ	C_L	C_η
0.22	1.4	1.9	0.4	0.65	1	1.3	1.2	6.0	0.36	85

2.2 Aerodynamic Coefficient

When looking at the aerodynamic aspects of ground vehicle, drag force, side force and lift force are always concerned. However, it would be more comprable to have the normalized force coefficients are defined as

$$C_d = \frac{F_d}{\frac{1}{2} U_\infty \rho A_x} \quad (2.2.1)$$

$$C_s = \frac{F_s}{\frac{1}{2}U_\infty \rho A_y} \quad (2.2.2)$$

$$C_l = \frac{F_l}{\frac{1}{2}U_\infty \rho A_z} \quad (2.2.3)$$

Where $F_{d,s,l}$ refer to the drag forces, side force, and lift force respectively, and $A_{x,y,z}$ is the projected surface area in the x-,y-, and z-direction respectively. ρ is the free stream fluid density, and U_∞ is the free stream velocity. $C_{d,s,l}$ is referred to as the drag coefficient, side fore coefficient, and lift coefficient.

Moreover, for truck aerodynamic performance investigation, yaw moment which is the moment around vertical axis and the roll moment around the horizontal axis, are considered.

2.3 CFD Coefficient

The dimensionless wall normal distance y^+ for a wall-bounded flow can be defined in the following way:

$$y^+ = \frac{u_* y}{\nu} \quad (2.3.1)$$

where y is the distance to nearest wall, ν is the the local kinematic viscosity of the fluid, and u_* is the friction velocity at the nearest wall defined by :

$$u_* = \sqrt{\tau_w / \rho} \quad (2.3.2)$$

where τ_w is the wall shear stress defined by:

$$\tau_w = \mu \left(\frac{\partial u}{\partial y} \right)_{y=0} \quad (2.3.3)$$

the Courant-Friedrichs-Levy (*CFL*) number is used to judge the quality of the mesh. In order to reslove the flow and transfer the imformation correctly between time steps, the local *CFL* number should not exceed one expressed as the following:

$$CFL = \frac{u \Delta t}{\Delta x} \leq 1 \quad (2.3.4)$$

2.4 Hybrid wall treatment

Wall function for near wall treatment should be implemented when the mesh is not sufficiently resolved. In this case, the hybrid wall treatment proposed by Popovac and Hanjalic is used [6]. It should ensure a gradual change between the viscous sublayer formulation and the wall functions. For hybrid wall treatment, the expressions for velocity profile, wall shear stress and near wall dynamic viscosity are described below:

$$U^+ = y^+ e^{-\Gamma} + \left[\frac{1}{\kappa} \ln(Ey^+) \right] e^{-1/\Gamma} \quad (2.4.1)$$

$$\tau_w = \tau_w^\nu e^{-\Gamma} + \tau_w^t e^{-1/\Gamma} = \left(\mu e^{-\Gamma} + \mu_{w,P} \psi_P e^{-1/\Gamma} \right) \frac{U_P}{y_P} \quad (2.4.2)$$

$$\mu_w = \frac{\kappa \rho C_\mu^{1/4} k_P^{1/2} y_P}{\ln(E y_P^*)} = \mu \frac{y_P^*}{U_P^*} \quad (2.4.3)$$

where

$$\Gamma = \frac{0.01 y^{+4}}{1 + 5 y^+} \quad (2.4.4)$$

Similarly derived, the production of the turbulence kinetic energy near wall \mathcal{P}_P and the energy dissipation rate ε_P can be expressed as:

$$\mathcal{P}_P = -\overline{uv} \frac{\partial \bar{u}}{\partial y} = C_\mu^\zeta \zeta_P \frac{k_P^2}{\varepsilon_P} \left(\frac{\partial \bar{u}}{\partial y} \right)_P^2 e^{-\Gamma} + \frac{C_\mu^{3/4} k_P^{3/2}}{\psi_P \kappa y_P} e^{-1/\Gamma} \quad (2.4.5)$$

$$\varepsilon_P = \frac{2\nu k_P}{y_P^2} e^{-\Gamma_\varepsilon} + \frac{C_\mu^{3/4} k_P^{3/2}}{\kappa y_P} e^{-1/\Gamma_\varepsilon} \quad (2.4.6)$$

This wall treatment provides the standard wall function for the large values of y^+ as well as integration of equations up to the wall for the very small values of y^+ .

3 Method

To start a numerical simulation for a computational fluid dynamic case, one first has to prepare and clean up the surface mesh, create the computational domain (volume mesh), set up boundary conditions and numerical method for the specific cases. In this section, firstly, since this simulation is based on the experiment conducted in the wind tunnel, therefore the experimental scenario and the parameters used in simulation which are from the experiment will be described. Then the detail of the computational domain and boundary condition will be described. Moreover, the numerical setup will be described as well.

3.1 The wind tunnel experiment

3.1.1 RAUG wind tunnel

This experiment was conducted in the RAUG wind tunnel. The sketch of its section area can be seen below. A very important parameter for wind tunnel experiment is blocking factor which represents the blockage effects of the vehicle in wind tunnel. In this case, the reference area of the half-scaled Volvo truck is $2.68m^2$, thus the blocking factor is calculated: $B = Area_{truck}/Area_{windtunnel} = 2.68/32.34 = 0.083$.

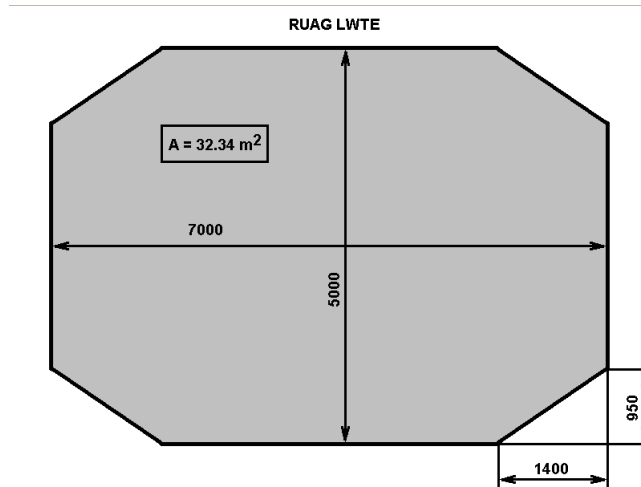


Figure 3.1.1: The sketch of the section area of the RAUG wind tunnel.

3.1.2 Experiment setup

The layout of the experiment can be seen in the Figure 3.1.2. As shown, the truck was put on turntable. Positive yaw angle is defined as when the right side of the truck model is the windward side. Moreover, the truck model was lifted 35mm above the floor due to its air cushion system. Additionally all the inlet speeds were measured 7.922m upstream from the turntable center and the moment-calculation reference point was set to 1.54m upstream from the turntable centre.

In this wind tunnel experiment, drag fore, side fore, lift force, the moment at X,Y,Z direction were measured respectively. The yawing speed of the truck is 0.15deg/s.

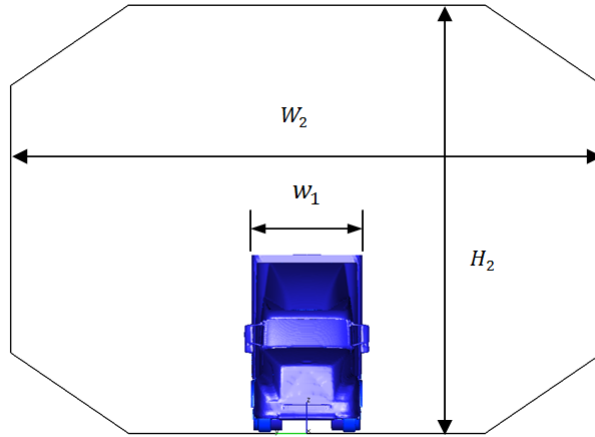


Figure 3.2.2: Sketch of the front view of computational domain.

Table 3.2.1: Parametres of the comutational domain.

Height of truck	$H_1 = 2.02m$
Length of truck	$L_2 = 9m$
Width of truck	$w_1 = 1.2m$
Distance from inlet to truck front	$L_1 = 8H = 16m$
Distance from truck rear to outlet	$L_3 = 15H = 30.3m$
Height of the wind tunnel	$H_2 = 5m$
Width of the wind tunnel	$w_2 = 7m$

3.3 Meshes

Some small parts of underbody geometry were taken away or slightly simplified in ANSA and AVL-Fire. Volume mesh was created using FAMEHexa, which is a automatic hexahedral cell mesh generator based on Octree method and packaged in AVL-Fire. In order to simulate truck oscillation, mesh deformation method was implemented. Thus several boxes around the truck model were created to get gradually-grown cell and decrease the number of needed cells. Additionally, the most inner box will rotate with the truck model during mesh-deforming process to keep the boundary layer and maintain the quality of these cells. Figure 3.3.1 shows a central cross section normal to Y axis. Figure 3.3.2 and 3.3.3 shows a cut of the mesh at the plane 0.8m above the ground for 0° yaw angle and 5° yaw angle for steady simulation respectively.

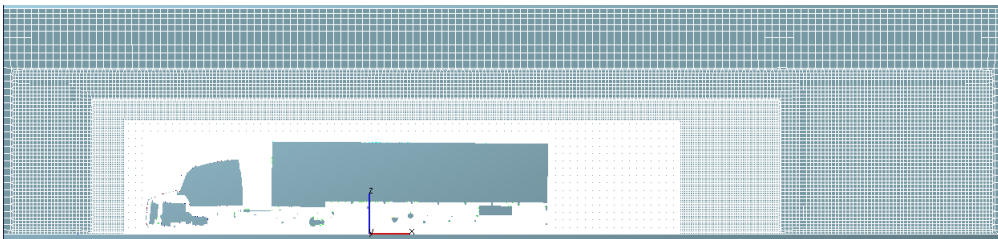


Figure 3.3.1: A central cut of the volume mesh from side view.

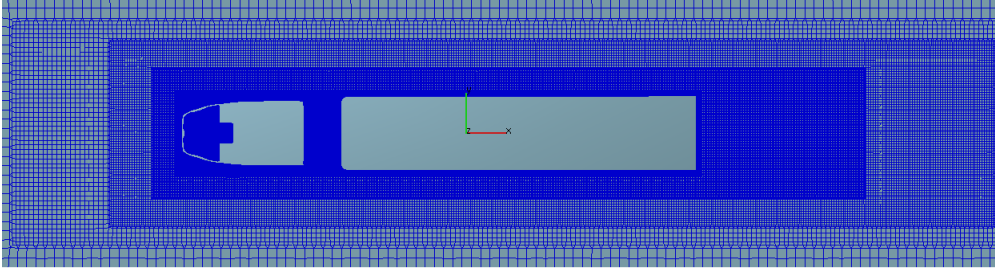


Figure 3.3.2: A cut of the volume mesh from top view at the plane $z = 0.8m$ for 0° yaw angle.

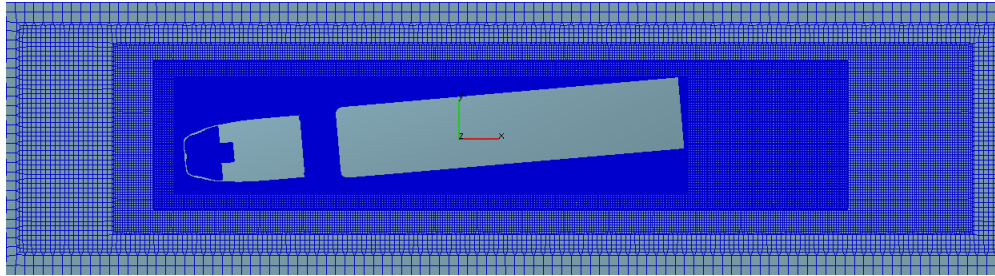


Figure 3.3.3: A cut of the volume mesh from top view at the plane $z = 0.8m$ for 5° yaw angle.

The oscillation of the truck model around the vertical axis is obtained by the setup of deforming the computational grid in the AVL-Fire solver. The initial volume mesh used for dynamic simulation is the same as the mesh for 0° yaw angle steady simulation. As mentioned, the cells within the most inner box is rotating with the truck. The effect of the mesh deformation at 1.6° yaw angle is illustrated in Figure 3.3.4.

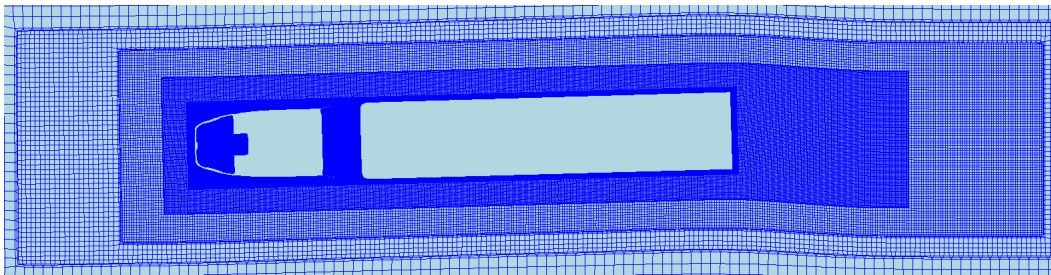


Figure 3.3.4: A cut of the deformed volume mesh at 1.6° yaw angle from top view at the plane $z = 0.8m$.

The meshes mainly consist of hexahedral cells. In 0° yaw angle steady simulation and dynamic simulation, a 44 million mesh is adopted. In 5° yaw angle steady simulation, a 49 million mesh is adopted. In the regions of important aerodynamic devices such as the tractor's roof and the side deflectors, the diffuser, where the geometry is thin and predictable separation occurs, massive small cells are used to resolve geometry and improve the robustness of the simulation. Additionally, a plenty of small cells are used to resolve the boundary lay in order to obtain a reasonable y^+ value to predict the separation correctly.

Hexahedral mesh is suitable for simulations with a dominant flow direction, which only applies if the faces are placed perpendicular to the flow. Therefore in the steady simulation for 5° yaw angle, instead of adjusting the direction of the inlet stream, the truck is rotated to 5 degree, and a bigger box is used to capture the wake at leeward side, see Figure 3.3.3. A zoom-in picture of the y-axis-normalized

cut of mesh at the roof deflector and trailer roof region can be seen in the Figure 3.3.5.

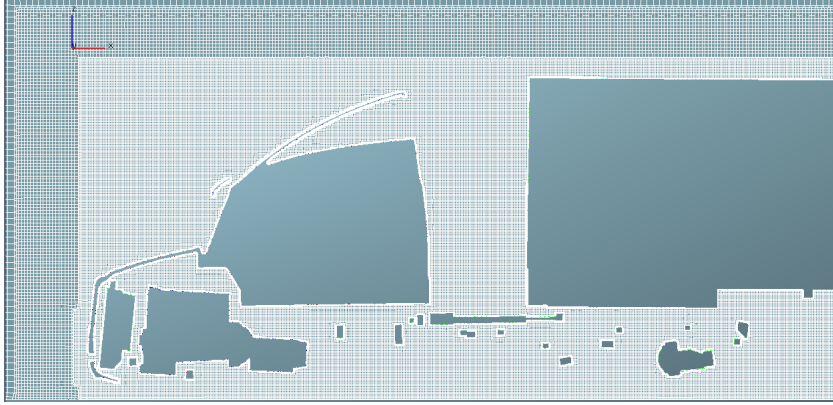


Figure 3.3.5: *Zoom-in in the roof deflector and trailer roof.*

3.4 Boundary condition and numerical setup

3.4.1 Boundary condition and initial condition

In the experiment, the truck model was put on the center of a turntable, and the floor of the wind tunnel was not moving. To modeling the flow in wind tunnel as accurate as possible, all solid surfaces including all parts of the truck and the surface of the wind tunnel were set to no-slip wall. The inlet of the computational domain was defined as Dirichlet boundary condition with a uniform normal velocity distribution profile. In dynamic simulation, the inlet speed is set to be $U_\infty = 33m/s$, in steady simulations, the experimental inlet speed $U_\infty = 50m/s$ is used. Moreover, the boundary condition for the outlet of domain was set to that all gradient equal to zero. All boundary conditions and initial condition are tabulated in the table 3.4.1 below.

Table 3.4.1: Boundary conditions and initial conditions

Boundary condition & Initial Conditon	Boundary sort	Value
Truck model	No-slip stationary wall	-
Wind tunnel floor	No-slip stationary wall	-
Wind tunnel surface	No-slip stationary wall	-
Wind tunnel inlet	Normal-velocity inlet	50 m/s (33 m/s)
Wind tunnel outlet	All gradient = 0	grad = 0
Turbulence level at inlet	-	0.003
Turbulence length at inlet	-	0.02m
Reference air density	-	1.205 kg/m^3
Reference air pressure	-	101399 pa

3.4.2 Simulations

All simulations are performed with the commercial software package AVL-Fire V2010.0. For the steady simulations, 5000 iterations are run. The the drag force and yaw moment are obtained by calculating the mean value of the last 100 iterations. For the dynamic simulation, the converged steady simulation result is used as initial condition, so as to reduce to computational time and improve

the convergence. Since the result from steady simulation is robust and may not represent the real flow, the mesh deformation is started at the 100th time step.

3.4.3 Numerical setup for CFD solver

For the transient simulation, second order time interpolation scheme was adopted. The time step was set to $\Delta T = 0.0001s$, so as to make the simulation stable in time, and make the CFL number smaller than 1 in most area of the computational domain. For both steady and transient simulations, $k - \zeta - f$ turbulence model was implemented, since it's fairly more robust and computational cheap than PANS and LES. Furthermore, it even can predict the stream more accurately when y^+ value is high in this case. For the discretization method, Mirror was set for calculation of boundary values; Least Sq.Fit was set for calculation of derivatives. For the differencing scheme, MINMOD Bounded which is a second order differencing scheme was set for momentum due to it's easy to converge. Second order central differencing was used for continuity, and Upwind was used for turbulence and energy. The convergence criteria were set to lower than 0.0001 for all normalized residuals. Additionally the under relaxation factors for the solved equations are listed in the table 3.4.2 below:

Table 3.4.2: Under relaxation factors for the solved equations.

Equation	Underrelaxation factor
Momentum	0.5
Pressure	0.3
Turbulence kinetic energy	0.2
Turbulence dissipation rate	0.2
Viscosity	1

4 Results

In section 4.1, wind tunnel experiment data are analyzed with simulation results. In section 4.2, steady simulation results for 0° and 5° yaw angle are described and analyzed. In section 4.3, the influence of the yaw motion of the truck on the flow field and furthermore on the aerodynamic performance of truck are illustrated.

4.1 Wind tunnel experiment data analysis with CFD results

Figure 4.1.1 shows the drag coefficient measured in the wind tunnel experiment, normalized by the measured C_d value at 0° yaw angle. The blue line corresponds to gradually decreasing yaw angle, and the red line corresponds to gradually increasing yaw angle. A fairly small phase shift can be observed at very small yaw angle close to 0 degree. Moreover, a difference of the measured drag coefficient exists between increasing and decreasing yaw angle. There's a critical value (around 1.5 degree) where the red curve intersects the blue curve. Before the critical angle, the measured C_d when the yaw angle is increasing is bigger than the measured C_d when the yaw angle is decreasing. After passing the critical yaw angle, the measured C_d when the yaw angle is increasing is smaller than the measured C_d when the yaw angle is decreasing. However, the difference is small due to the very small yawing velocity in the experiment.

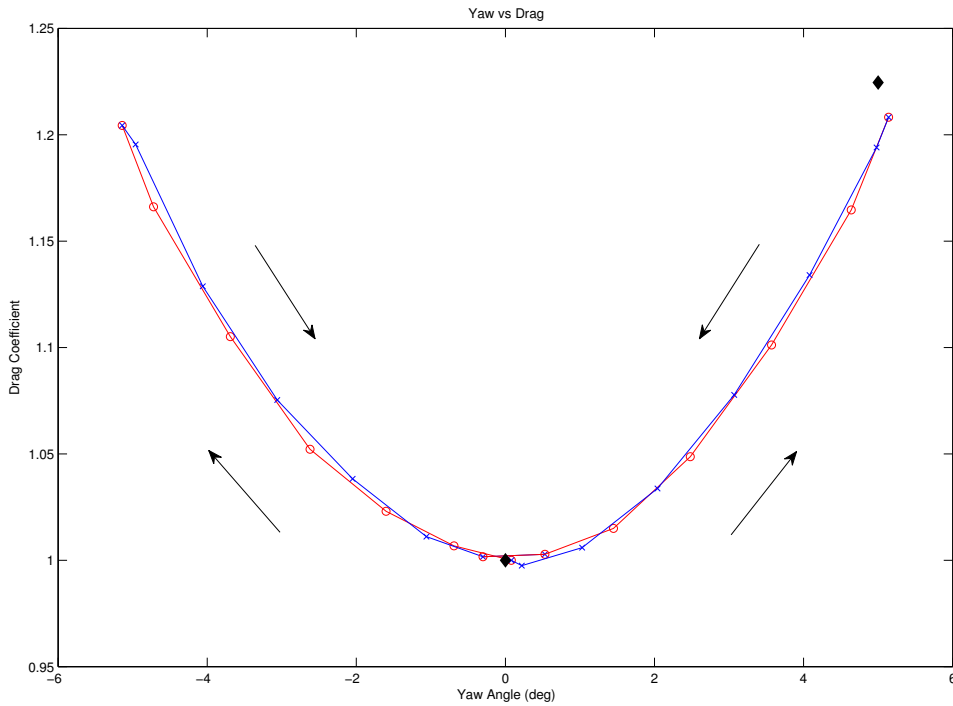


Figure 4.1.1: Drag coefficient vs. Yaw angle plotted from experiment data, normalized by the measured C_d value at 0° yaw angle. The black diamonds show the simulation results.

Figure 4.1.2 shows the measured yaw moment in the wind tunnel experiment. It can be found the measured yaw moment when the truck is rotating from -5° to 5° is higher than that when the truck is rotating from 5° to -5° .

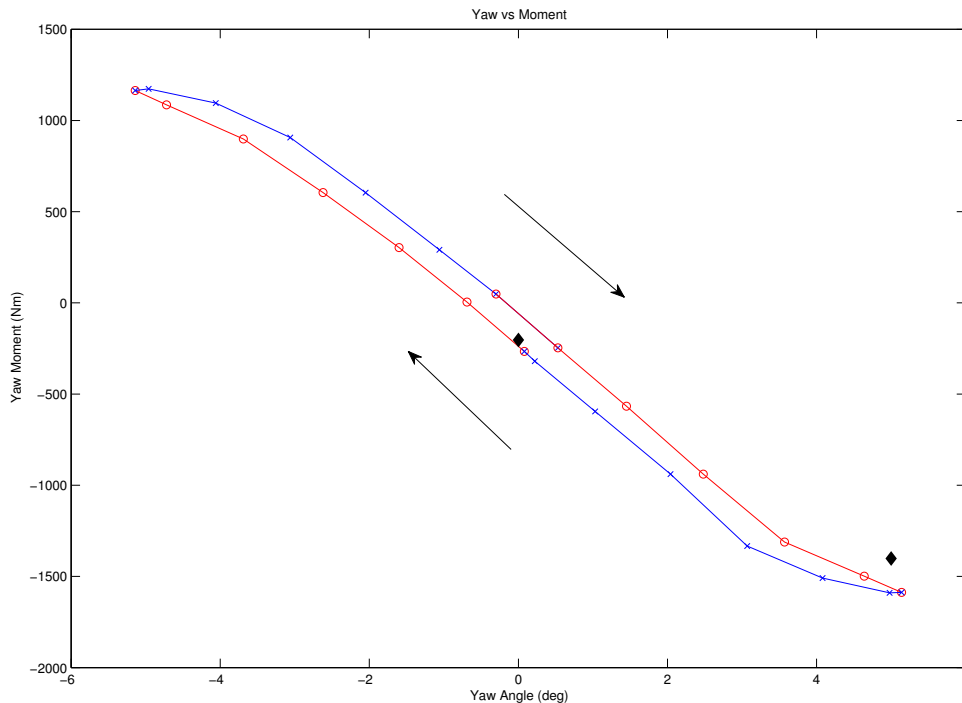


Figure 4.1.2: *Yaw moment vs. Yaw angle plotted from experiment data. The black diamonds show the simulation results.*

The phenomena mentioned above will affect the measurement. In order to obtain the genuine drag coefficient value, and to visualize the real flow field when the truck is stationary, two simulations for 0° , 5° degree yaw angle and with the inlet speed 50m/s are performed. The C_d values and yaw moment obtained from steady simulations are listed in the Table 4.1.1. They are pointed out in Figure 4.1.1 and Figure 4.1.2 by black diamond as well. As shown, the simulation result at 0° yaw angle agrees with the experiment measurement very well. While at 5° yaw angle, the simulation result differs with experiment measurement about 7 percent. Since the flow at the leeward side of the truck is far more turbulent at 5° yaw angle, this difference may due to the quality of the mesh at the leeward side of the truck. Improvement of the mesh and more iterations of simulation are required to improve the results.

Table 4.1.1: The Calculated C_d and yaw moment for 0° , 5° yaw angle compared with experiment measurement. C_d were normalized by measured C_d value at 0° yaw angle.

Yaw angle	0°	5°
Calculated C_d	1.00	1.21
Measured C_d	1.00	1.19
Calculated yaw moment	-184.4Nm	-1451.7Nm
Measured yaw moment (from -5° to 5°)	-58.3Nm	-1562.5Nm
Measured yaw moment (from 5° to -5°)	-237.5Nm	-1594.5Nm

4.2 Numerical simulation results for stationary truck at 0° and 5° yaw angle

4.2.1 Overview of the flow field

Although the instantaneous flow around truck is highly turbulent and chaotic, truck's aerodynamic performance is dominated by large turbulence structure, for instance, the wake behind the truck. In Figure 4.2.1, velocity magnitude at central cross section with streamlines is shown. The turbulence structure of the wake with low speed can be obviously seen behind the trailer. As seen, there mainly are two swirls behind the trailer. The upper swirl is created by the high speed air flow passing along the roof of the trailer. The lower swirl is created by the underbody air flow which suddenly exits to a large area. Moreover, it can be seen that the flow underbody is accelerated by the diffuser significantly. And it leads to highly turbulent flow at engine compartment.

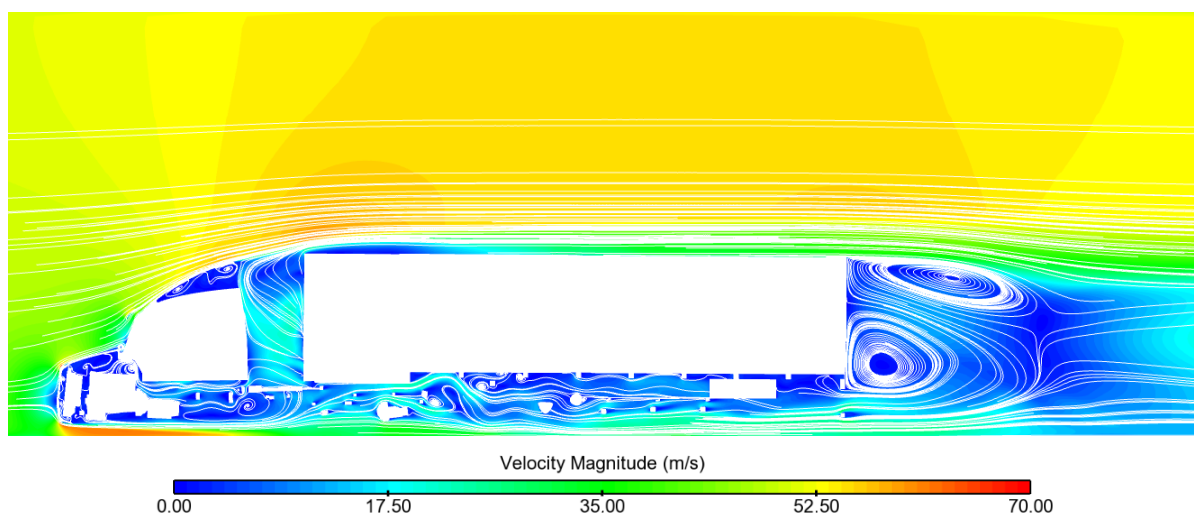


Figure 4.2.1: *Velocity magnitude at central cross section with streamlines.*

The pressure coefficient at central cross section is demonstrated in Figure 4.2.2. As shown, a low pressure region is created behind the trailer due to the air flow sucked into the wake from sides. Another two low pressure regions are observed at the front edge of trailer and at the trailing edge of deflector. The low-pressure region at the front edge of trailer is caused by the wake generated when flow separates at the trailing edge of the deflector. And the low pressure region at the trailing edge is caused by the acceleration of the flow around the wake. Small vortex in the wake can be seen at this area in Figure 4.2.1.

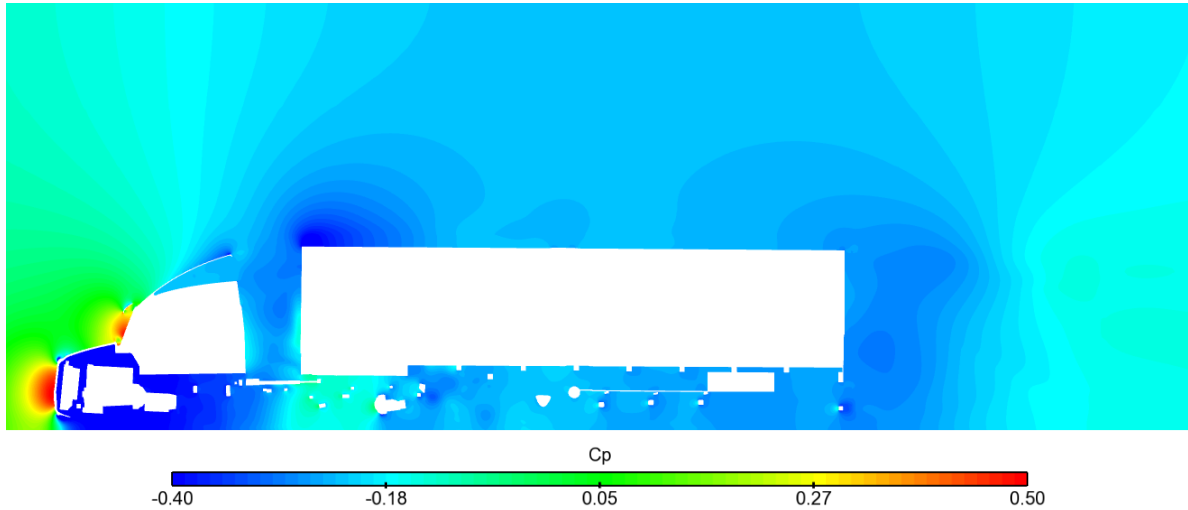


Figure 4.2.2: *Pressure coefficient at central cross section.*

Furthermore, different wake structures at spanwise direction are created at different yaw angle. Velocity magnitude with streamlines at the plane 1100mm above the ground are displayed for 0 degree and 5 degree yaw angle respectively in Figure 4.2.3. At 0 degree yaw angle, two symmetric swirls can be found behind the trailer, created by the flow separating at the trailing edge of two lateral side of the trailer respectively. However, at 5 degree yaw angle, the swirl at leeward side is bigger than the other one. It's because more air flow coming through the tractor-trailer gap is separated at the leeward side into an enlarged area. Moreover, two almost symmetric swirls can be found in the gap between the tractor and the trailer at 0 degree yaw angle, while at 5 degree the swirl at leeward side almost disappears. It's because air flow entre the gap from windward direction. As seen, the flow at the gap is strongly turbulent and irregular, thus it will be studied further later.



(a) 0° yaw angle



(b) 5° yaw angle

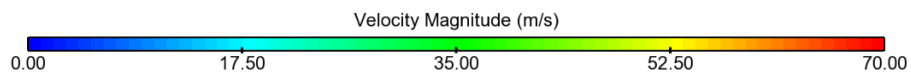


Figure 4.2.3: *Velocity magnitude with streamlines at the plane 1100mm above the ground*

The low pressure region at the wake is important for drag production, therefore a further insight is taken on the rear of the trailer. In Figure 4.2.4, the pressure coefficient on the rear of the trailer is shown for 0 degree and 5 degree yaw angle respectively. The high pressure center indicates the border of the two swirls. At 5 degree yaw angle, the high pressure center shift to left because the right swirl is expanded. And this high-pressure-center-shift also contributes to yaw moment generation. Figure 4.2.4 also shows how significantly the pressure decreases on the rear surface of the trailer at cross-wind condition, which contributes to drag increase.

In figures 4.2.5 and 4.2.6, the isosurface of total pressure equal to zero colored by pressure coefficient is displayed for 0 degree and 5 degree yaw angle respectively. Large wake structure appears around and behind the truck for both cases. These unsteady wake structures represent large energy losses in the flow which contributes to drag production. As seen, at 0° yaw angle, the wake is almost symmetric. Additionally, it can be observed that the flow separate after passing the front deflector and then reattach the trailer roof until it reaches the rear edge of the trailer roof where the air separate again

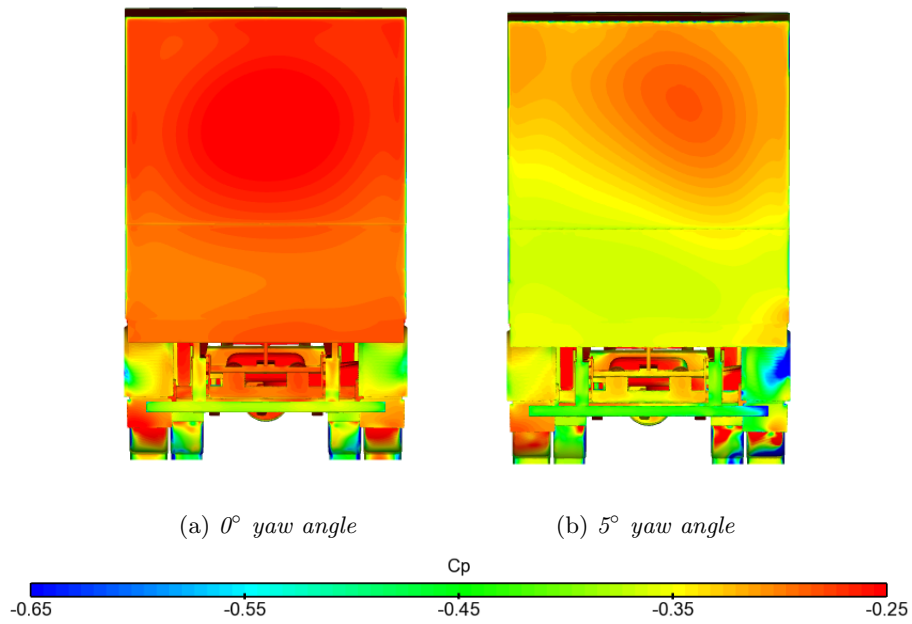


Figure 4.2.4: *Pressure coefficient on the rear surface of trailer.*

and a large base wake is generated. Moreover, a flow loss after the two mirrors and above them which is originated from the sun visor can be seen as well.

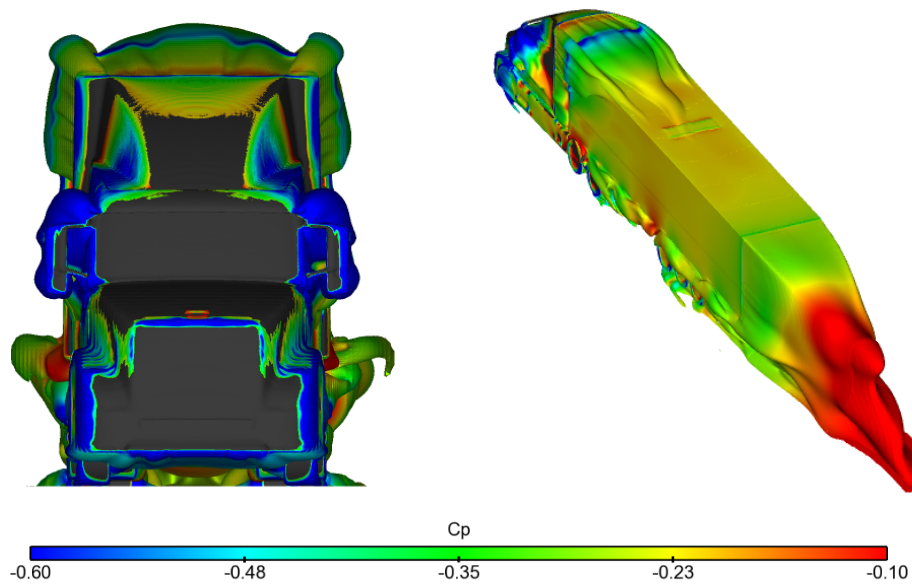


Figure 4.2.5: *Isosurface of total pressure equal to zero at 0° yaw angle.*

At 5° yaw angle, a larger asymmetric wake structure is created at the leeward side, which refers to larger flow energy losses leading to a larger drag production.

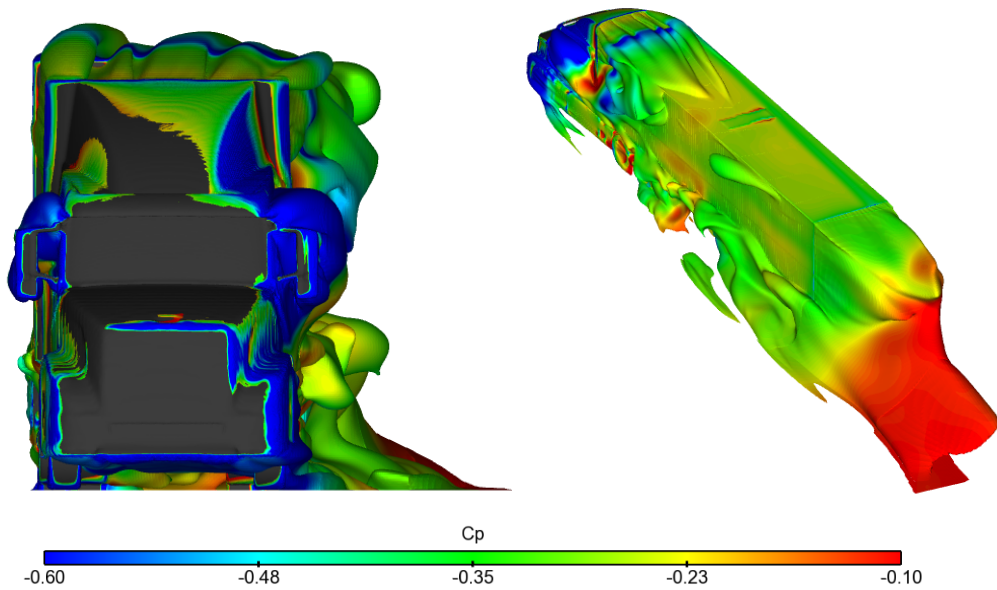


Figure 4.2.6: *Isosurface of total pressure equal to zero at 5° yaw angle.*

Besides large turbulence structures, relative small vortices also affect the flow and further affect the aerodynamic performance. Moreover, the amount of the flow structure that has been modelled by the chosen turbulence model is also of interest. A way to visualize these rotational structures is the isosurface of Q invariant. Figure 4.2.7 shows the isosurface of the second invariant of velocity gradient equal to 3000 for 0 degree and 5 degree yaw angle. As seen, in contrast to 0 degree yaw angle, at 5 degree yaw angle, the flow is much more turbulent in the wake behind the trailer and at leeward side of the underbody. Additionally, at 5 degree yaw angle, a long leading-edge vortex structure can be observed above the lateral edge of the trailer at windward side. It's created by the flow hitting the windward lateral surface of the trailer and climbing over the roof edge.

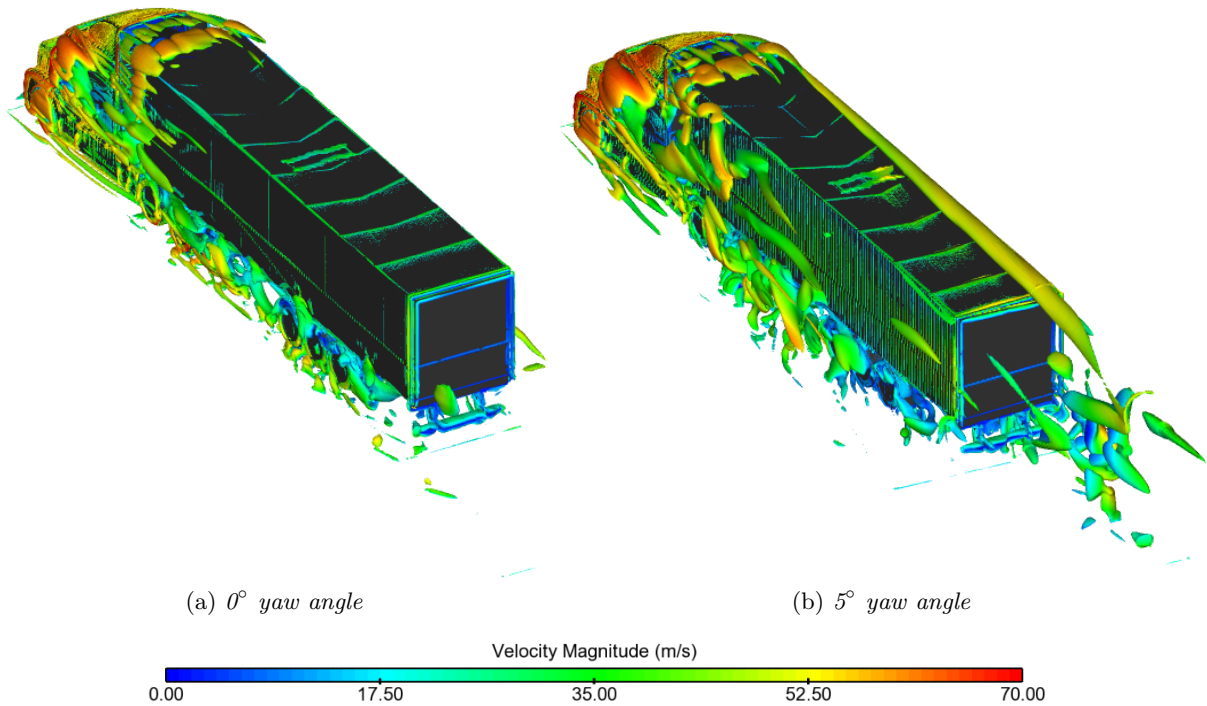
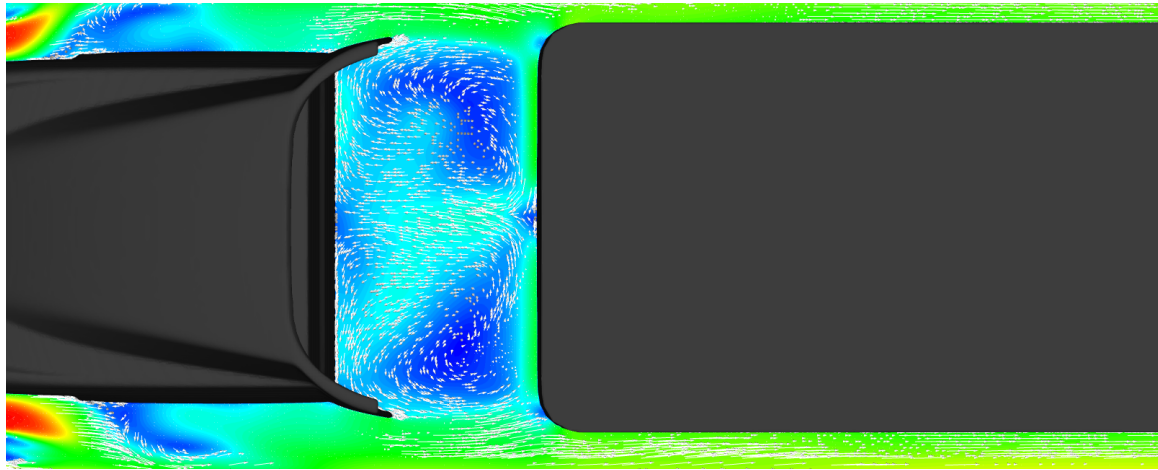


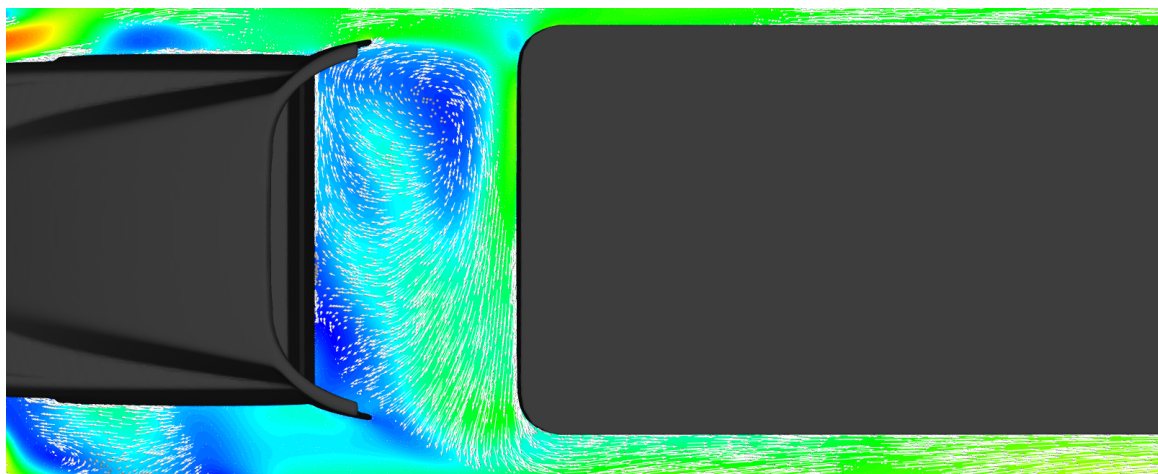
Figure 4.2.7: *Isosurface of the $Q = 3000$ colored by velocity magnitude.*

4.2.2 Flow in the gap between tractor and trailer

The flow in the gap between the tractor and the trailer is strongly turbulent. A velocity magnitude with velocity vector at the plane 1100mm above the ground are shown in Figure 4.2.8. A large amount air come out of the engine compartment at both cases. However at 5 degree yaw angle, besides the flow from the engine compartment, the flow from the windward direction blow into the gap. The flow exits from the other side and attach the leeward lateral surface of the trailer until it separates at the trailing edge of the trailer.



(a) 0° yaw angle



(b) 5° yaw angle

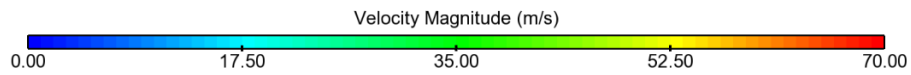


Figure 4.2.8: Velocity vector in the gap between the tractor and the trailer at plane 1100mm above the ground.

The pressure coefficient on the front surface of the trailer is displayed for 0 degree yaw angle and 5 degree yaw angle respectively in Figure 4.2.9. As seen, at 0 yaw angle, no high pressure region can be found on the upper edge of the trailer. This indicates no flow separating from the deflector of the tractor hit the trailer, which further means the deflector works well on drag reduction. Additionally, at 0 degree, relative high pressure areas appear at two side edge and the lower center of the trailer front. It corresponds to the area where the flow from the engine compartment hit the trailer. Moreover, at 5 degree, high pressure peaks at the windward edge of the trailer front. And in contrast to 0 degree, a low pressure region can be found at the leeward side edge, corresponding to the area where flow accelerate and exit the gap.

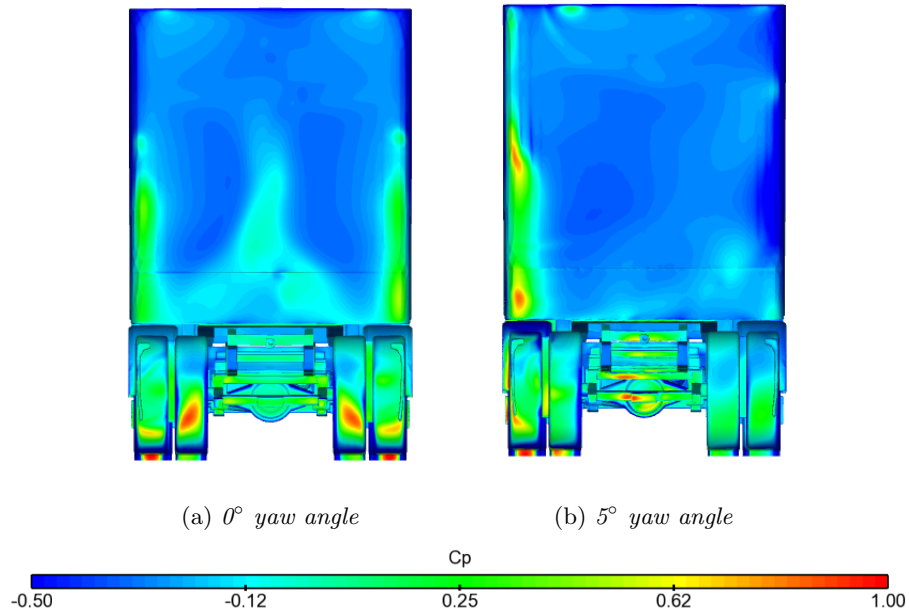
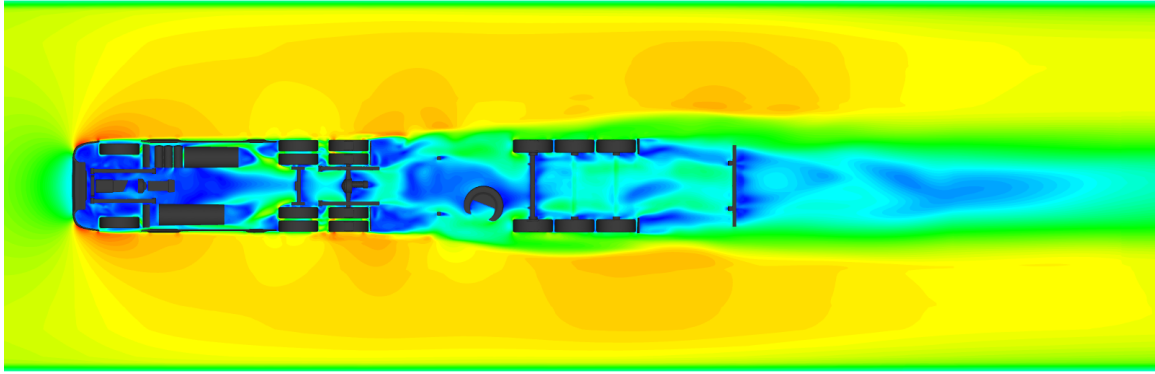


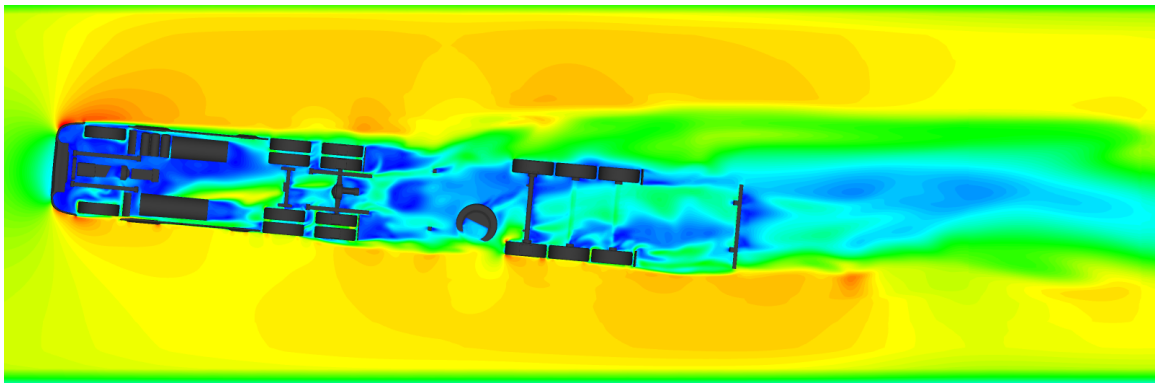
Figure 4.2.9: *Pressure coefficient on the front surface of trailer.*

4.2.3 Underbody flow

Velocity magnitude at the plane 285mm above the ground is displayed in Figure 4.2.10. As seen, the underbody flow is strongly separated and turbulent due to the disturbances of the complex geometry. At 5 degree yaw angle, the flow is more disturbed. And large amount cross-wind enters the underbody and exits from the other side. While at 0 degree yaw angle, most air exit from rear. This difference changes the wake structure behind trailer.



(a) 0° yaw angle



(b) 5° yaw angle

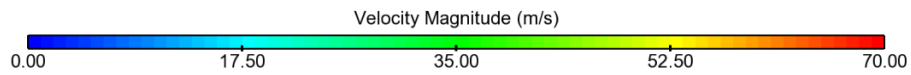
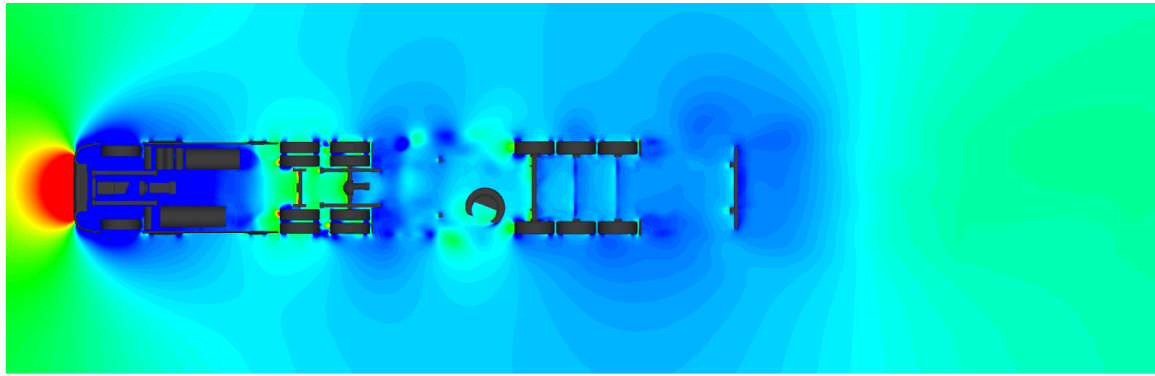
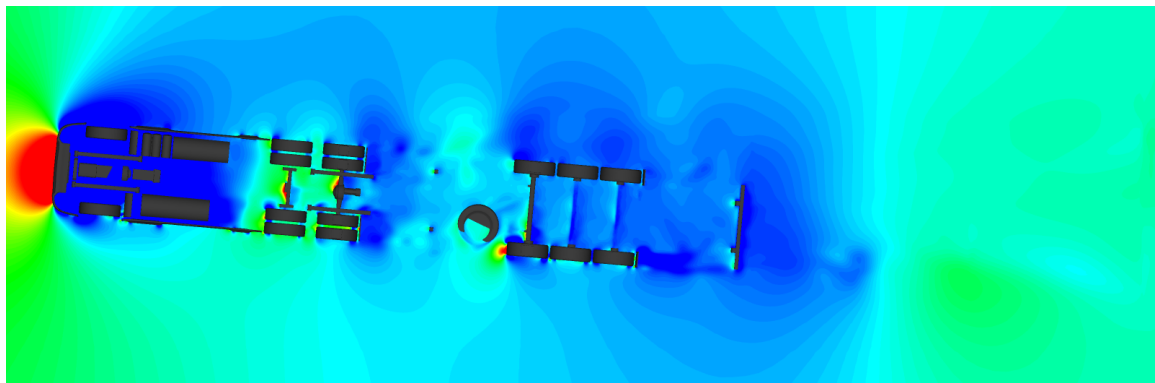


Figure 4.2.10: *Velocity magnitude at plane 1100mm above the ground.*

Pressure coefficient at the plane 285mm above the ground is displayed in Figure 4.2.11. Both at 0 and 5 degree yaw angle, a pressure transient can be found in the area between the engine compartment and the undercarriage. This is because large amount of the flow from engine compartment exit to the gap between the tractor and the trailer, rather than flow into the undercarriage.



(a) 0° yaw angle



(b) 5° yaw angle

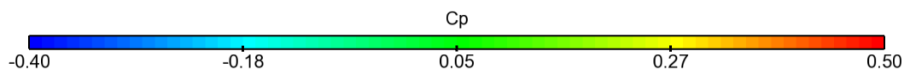


Figure 4.2.11: *Pressure coefficient at plane 1100mm above the ground.*

4.3 Comparison between stationary and rotating cases

As seen in the previous pictures, in contrast to steady condition, for the same yaw angle at dynamic condition, the drag force and yaw moment is different between the case when yaw angle is gradually increasing and the case when yaw angle is gradually decreasing. The reason why this phenomenon happens is that the flow around the truck is changed by its yaw motion. In the following section, the air flow around the truck at 1.6 degree yaw angle is compared between steady condition and dynamic condition. Furthermore, its influence on the aerodynamic performance is analyzed as well.

Firstly, a direct impression about how the flow around the truck is changed by its yaw motion can be given by the visualization of the streamlines. Streamlines are released from the same plane located at the rear of the trailer, and they are shown in Figure 4.3.1 for steady and dynamic condition respectively, colored by velocity magnitude. As seen, the direction in which the coming flow hit the tractor is changed. Moreover, the flow at the two lateral side of the truck is also twisted by the truck's yaw movement. It can be seen that the air flow on the leeward side reattach the left lateral surface of the trailer later in dynamic condition. Additionally, on the windward side the flow separate the right lateral surface of the trailer earlier in dynamic condition. These phenomena will lead to a change of pressure on the two side surface of trailer. Furthermore, it can be seen that the flow at leeward side passing over the trailer is suddenly sucked into the wake behind the trailer, creating a vortex behind the left edge of the trailer rear. It is due to the air flow is pushed and move with the rotating rear surface of the trailer.

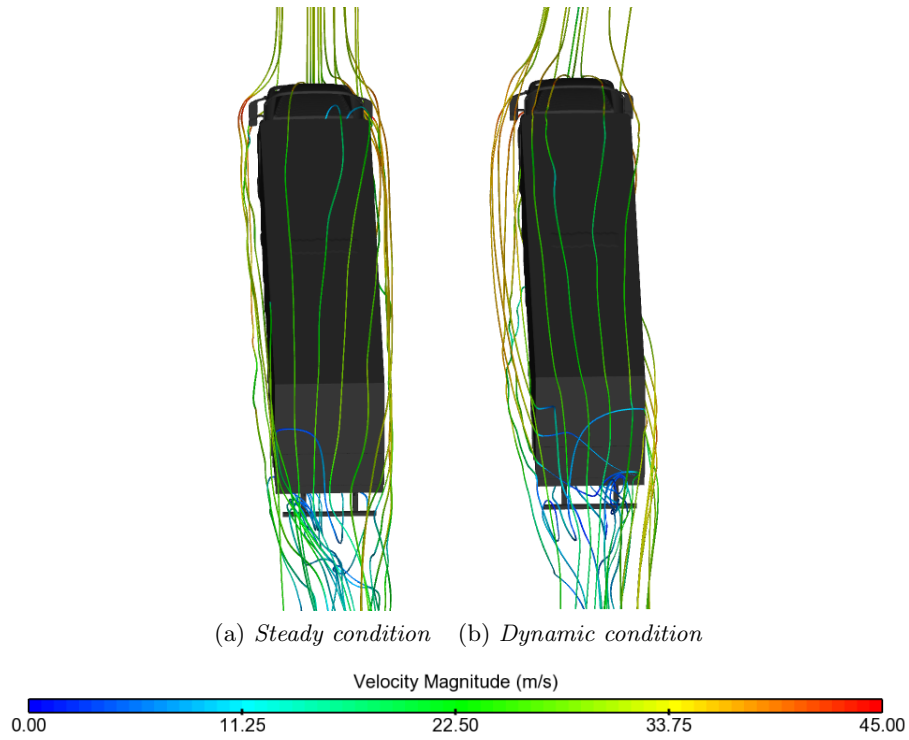


Figure 4.3.1: *Streamlines around the truck at 1.6 degree yaw angle.*

The vortex mentioned above also can be seen in Figure 4.3.2 showing the second invariant of velocity gradient $Q = 3000$, and another similar vortex structure can be seen behind the right edge also created by the rotating motion of the rear surface of the trailer.

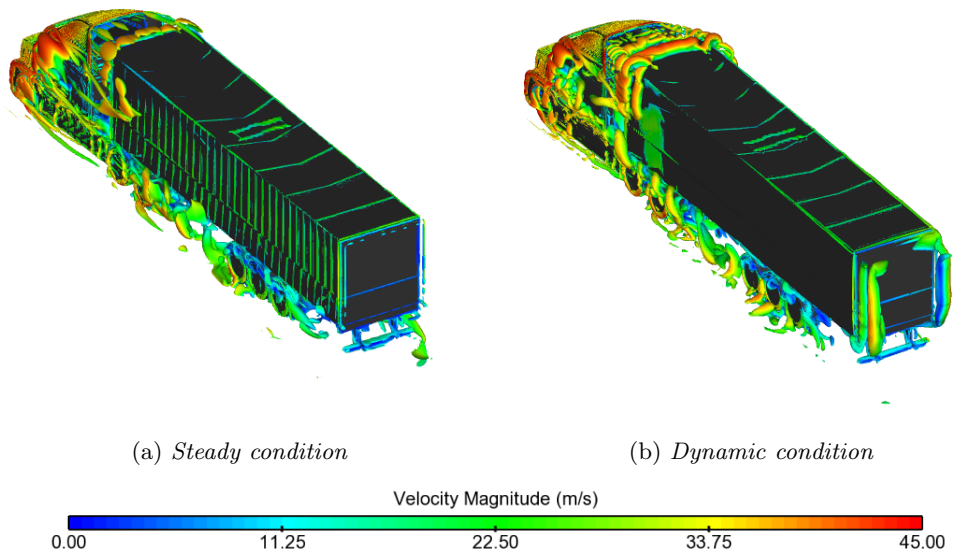


Figure 4.3.2: *The second invariant of velocity gradient $Q = 3000$ at 1.6 degree yaw angle, coloured by velocity magnitude.*

As mentioned before, the wake behind the trailer has a big influence on the truck's aerodynamic performance. Therefore a further analysis on the wake structure is employed. Figure 4.3.3 shows the isosurface of total pressure equal to zero for steady and dynamic condition respectively. As seen, at dynamic condition the wake has a shift to adjust to the direction of rotation compared to that at steady condition. It is due to the separation of the flow on the lateral surface at windward side is earlier, while on the leeward side it is retarded, see Figure 4.3.1. Moreover, it can be seen that the pressure of the vortex behind the truck rear on the leeward side is increased; while on the windward side is decreased. This is because, on the leeward side the air flow is pushed, but on the windward side the air flow is dragged, as a result of the different speed direction of the truck motion on these two sides.

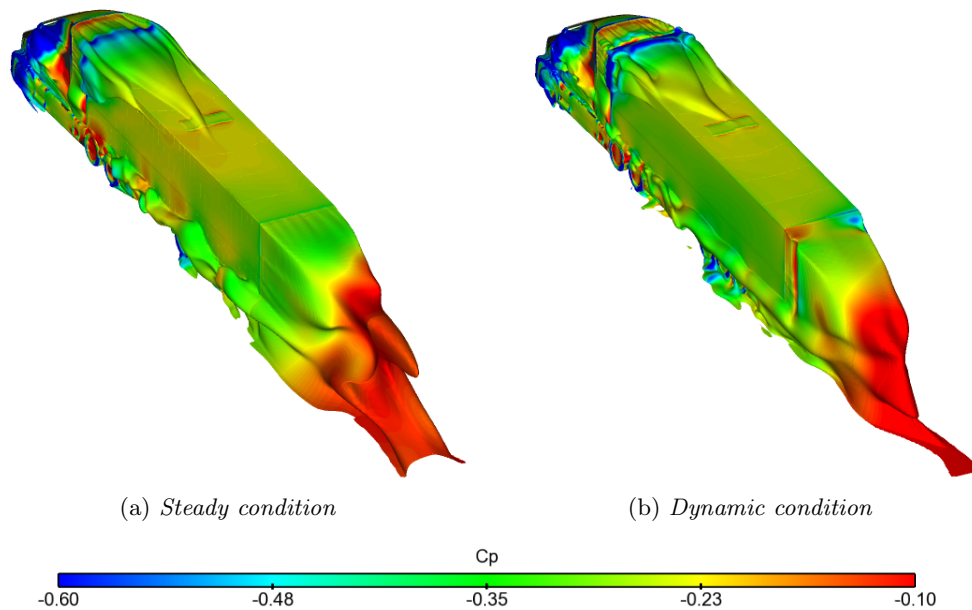


Figure 4.3.3: *The isosurface of the total pressure equal to zero at 1.6 degree yaw angle, coloured by pressure coefficient.*

Since the trailer has a large lateral surface, the change of the air flow on the two sides is further dig. Figure 4.3.4 shows the velocity magnitude with streamlines at the plane 1100mm above the ground for steady and dynamic condition respectively. The earlier separation on the windward side and retarded reattachment can be clearly observed. It also can be observed that the two big swirls behind the trailer at steady condition are squeezed by two newly created vortex mentioned above.

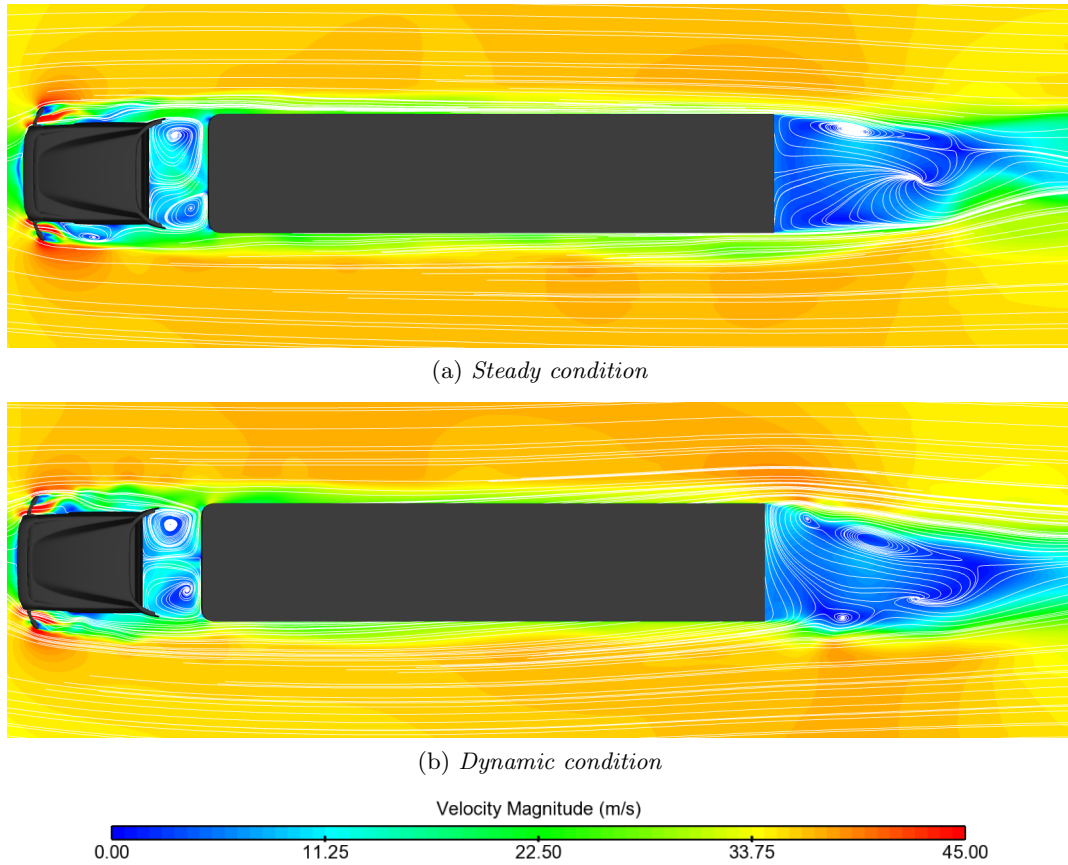


Figure 4.3.4: *Velocity magnitude with streamlines at the plane 1100mm above the ground.*

The change of pressure at the area of the two newly created vortex also can be seen in the Figure 4.3.5. Moreover, the pressure wave caused by the rotation motion of truck can be seen as well.

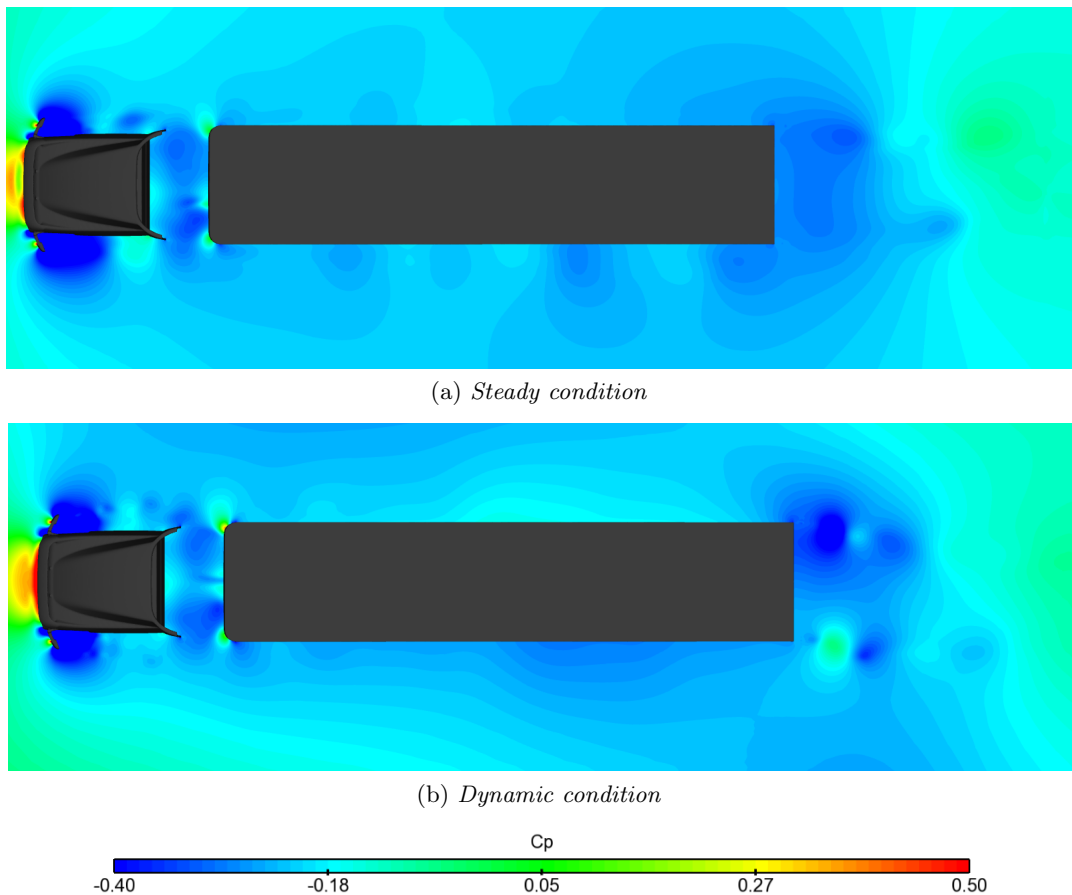


Figure 4.3.5: *Pressure coefficient at the plane 1100mm above the ground.*

So far it's known that there are several factors will influence the aerodynamic forces, such as the change of the separation of flow on the two lateral side of trailer and the change of the wake behind the rear of the truck. How and how much have these factors affected the drag production is studied in the following content.

Figure 4.3.6, 4.3.7, 4.3.8, 4.3.9 show the pressure coefficient value on the four surfaces of the trailer at steady and dynamic condition respectively. At dynamic condition, from Figure 4.3.6, it can be seen that a big high pressure region appears on the left side of the rear surface which will increase the drag. While on the right side the pressure decreases a lot, which will decrease the drag. The total influence of these two opposite effects is calculated later. From Figure 4.3.6, it can be seen that two relative high pressure region appears on the upper edge the trailer front. This indicates the region where the flow separating from the deflector hit the trailer. However, no big difference from two cases is observed, thus its effect on drag changes is not calculated later. From Figure 4.3.8, 4.3.9, the effect of the yaw motion on the two lateral surface of the trailer can be clearly observed. At dynamic case, the pressure on the windward side is increased, and the pressure on the leeward side is decreased, and this leading to a drag reduction, and the yaw-moment reduction as well. In order to evaluate these effects by quantity, the X components of the force calculated by integrating the pressure on these surfaces are listed in the table below. Thus it can be seen that the drag increase gaining by the pressure change the rear surface of the trailer is bigger than the drag decrease gaining by the pressure

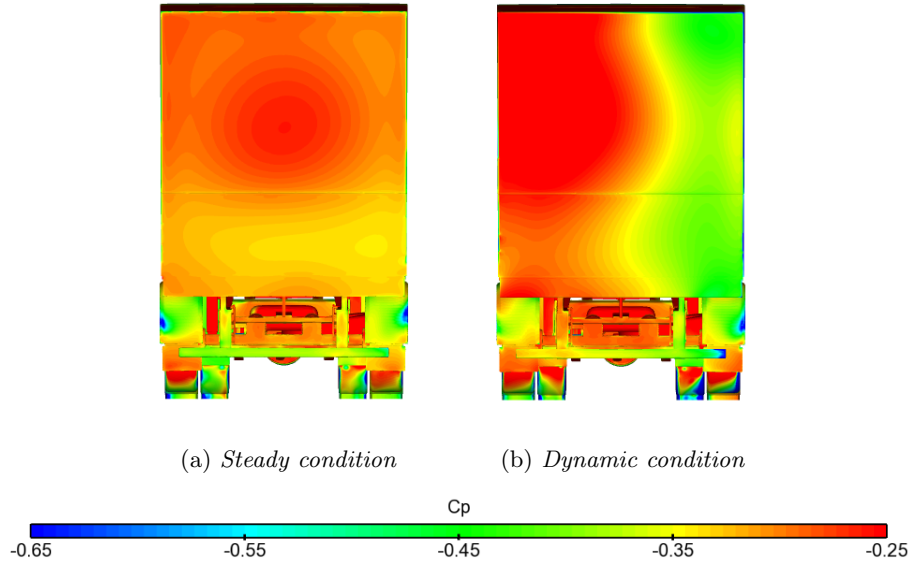


Figure 4.3.6: *Pressure coefficient at the rear surface of the trailer.*

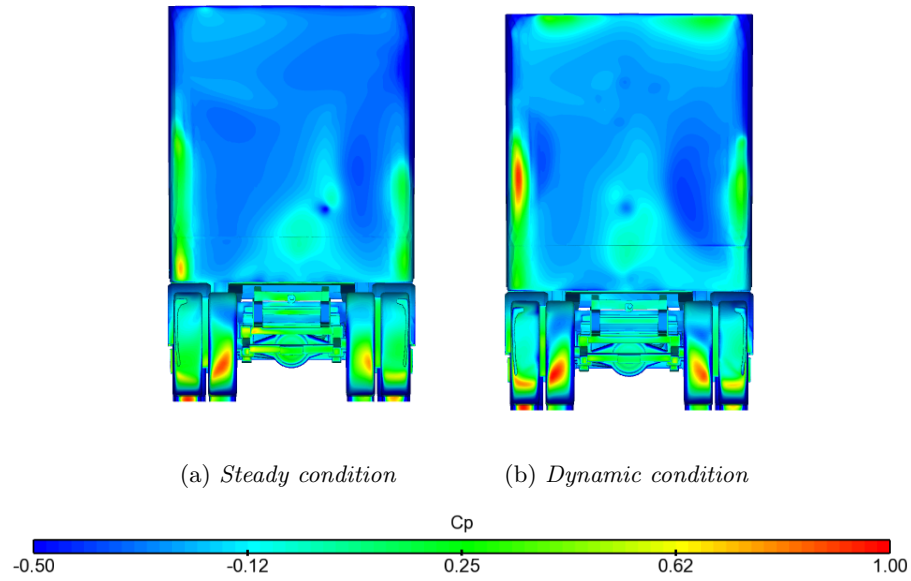
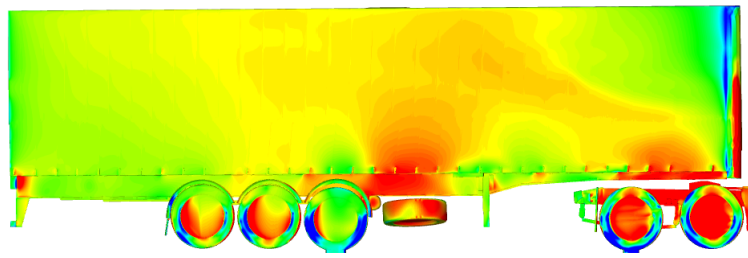


Figure 4.3.7: *Pressure coefficient at the front surface of the trailer.*

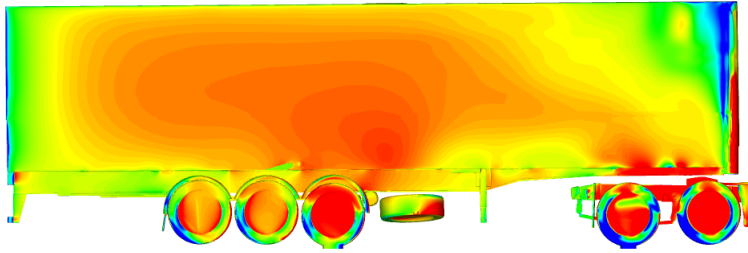
change on the two lateral surface of the trailer. It's because at small yaw angle and with high yaw speed, the pressure on the rear surface increase dramatically, however the X component of the force on lateral surface is relative small compared to the force on the rear surface.

Table 4.3.1: The X component of the force the two lateral and the rear surface of the trailer.

Surface	rear	windward	leeward
Steady condition	211847.5N	24683.7N	24395.1N
Dynamic condition	211945.5N	24708.4N	24375.9N
Difference	102N	24.7N	-19.2N



(a) *Steady condition*



(b) *Dynamic condition*

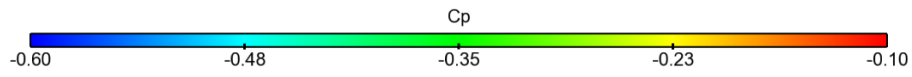
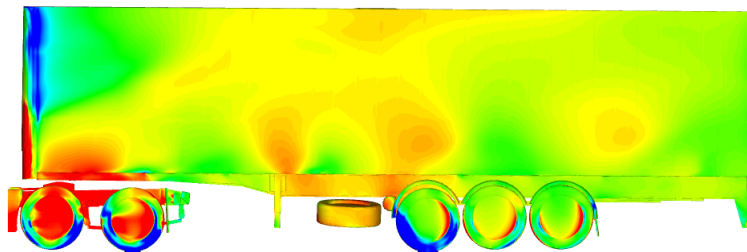
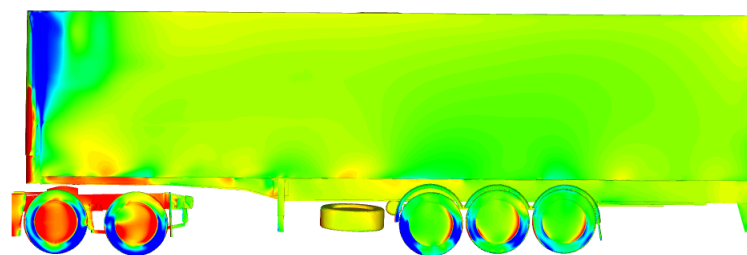


Figure 4.3.8: *Pressure coefficient at the windward side lateral surface of the trailer.*



(a) *Steady condition*



(b) *Dynamic condition*

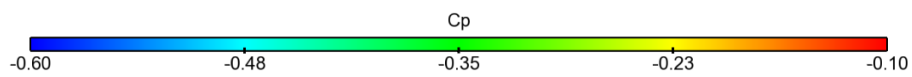


Figure 4.3.9: *Pressure coefficient at the leeward side lateral surface of the trailer.*

5 Discussion and Conclusion

The difference of the air flow around the truck between steady condition and dynamic condition is explained in Chapter 4. Firstly the wake structure behind the trailer is different. Two vortices are created by the rotating motion of trailer's rear surface. Additionally, earlier flow separation on the windward side surface of trailer and hysteresis of the flow reattachment on the leeward side surface of trailer are found due to the centrifugal force caused by the truck's rotating motion. Furthermore, these differences of flow structure lead to the change of pressure on the surface of the truck resulting in the change of aerodynamic forces and yaw moment. Therefore these changes of the flow structure and pressure on the truck's surface is the important causes of the difference in drag experimental measurement. In this specific case (1.6 degree yaw angle with 2Hz rotating frequency and 33m/s inlet speed), the drag increased by the pressure change at rear surface of the trailer is bigger than the drag decreased by the pressure change at the two lateral surfaces of the trailer.

However, due to limited time and computational power, a high frequency of yawing and a lower inlet speed were used in the compared simulations. From the results obtained from the simulations, it is found that there are four factors affecting the difference of measured drag between increasing yaw angle and decreasing yaw angle: yawing velocity, inlet speed, yaw angle, and the geometry of the truck.

Several predictions can be made. First, at lower yawing velocity, the change of the flow field and pressure on the truck is smaller, therefore the observed difference on the Drag-Yaw Angle curve will be smaller. Second, with higher inlet speed, the pressure change on rear surface would be smaller, while the pressure change on the two lateral surface would be bigger. This will decrease the critical yaw angle observed in the experimental measurement. Furthermore, the yaw angle is very important influential factor. As the yaw angle increases, the high pressure region observed on the rear surface will shrink and finally vanish, while the low pressure region on the rear surface will expand. Additionally the X component of the force generated by the pressure change would be bigger, since the angle between the flow and lateral surface is bigger. Finally the geometry also will influence the Drag-Yaw Angle curve, not only because different geometry will lead to different flow field, but also it will change the size of the area where the pressure change is integrated. Nevertheless, these predictions should be verified by CFD simulations in the future.

It also can be concluded that numerical simulation is very useful to predict the drag coefficient and reveal the air flow field for steady condition in this case.

References

- [1] S. Girimaji. “Partially-Averaged Navier-Stokes model for turbulence: Implementation and Validation”. In: *43rd AIAA Aerospace Sciences Meeting and Exhibit*. Notes on Numerical Fluid Mechanics and Multidisciplinary Design 10-13 January, Reno, Nevada (2005).
- [2] P. Cillieron, F. Chometon, and J. Laurent. “Analysis of hysteresis and phase shifting phenomena in unsteady three-dimensional wakes”. In: *Experiments in Fluids* 35 (1995), pp. 117–129.
- [3] S. Watkins and J. Saunders. “Turbulence experienced by road vehicles under normal driving conditions”. In: *SAE 950997* (1995).
- [4] S. Krajnovic, A. Bengtsson, and L. Davidson. “Numerical study of crosswind stability of a simplified at gust wind”. In: *8th MIRA International Aerodynamic Conference* (2010).
- [5] M. Popovac and K. Hanjalic. “A robust near-wall elliptic-relaxation eddy-viscosity turbulence model for CFD.” In: *INTERNATIONAL JOURNAL Heat and Fluid Flow* 25 (2004), pp. 1047–1051.
- [6] M. Popovac and K. Hanjalic. “Compound Wall Treatment for RANS Computation of Complex Turbulent Flows and Heat Transfer”. In: *Flow, Turbulence and Combustion* 45 (1997), pp. 1137–1159.